ARKIV FÖR FYSIK Band 3 nr 24

Communicated 24 January 1951 by G. Borelius and H. Alfvén

Notes on the focusing properties of homogeneous magnetic sector fields

By Rolf Persson

With 13 figures in the text

Introduction

Wedge-shaped homogeneous magnetic fields have been used in mass spectrometers for more than ten years. It is well known that the most commonly used arrangement with straight field boundaries and with the ion beam crossing these boundaries perpendicularly gives only first-order focusing. In recent years several authors have treated the problem of improving the focusing either by giving the field boundaries appropriate shapes or by changing the geometry. Bainbridge [1] has given formulae to obtain second-order focusing with circular boundaries. Hintenberger [2–4] has developed a general theory of the second-order focusing when using uniform magnetic fields and has given the field shapes for perfect focusing. Kerwin [5] has also treated the problem, especially for straight field boundaries in a symmetrical arrangement. He has also built an instrument according to these principles [7]. Spighel [8] has presented a theory, which, however, is not generally applicable. Some asymmetrical cases have been calculated by Kerwin and Geoffrion [6], although their results may not be correct in all cases (see p. 462).

This article will discuss some special focusing problems of homogeneous magnetic fields. In Chapter I the graphical construction already shown by Cartan [9] has been used for two purposes:

1) to find the locus of the foci for varying masses, which locus may be of interest for the alignment of multiple collectors [10] and of photographic plates [11], and
2) to show the aberration of different field arrangements, giving first-, second- and third-order focusing.

The problem of the third-order focusing will be discussed to some extent. To obtain numerical values of the aberration and the dispersion the graphical construction is not appropriate. Therefore the focusing conditions will also be treated analytically. The treatment is mainly restricted to some symmetric fields with straight and circular boundaries, which cases may be of practical interest. The different field arrangements will be compared as to aberration, dispersion and resolving power. Finally, in Chapter II we will describe a particular instrument, constructed to give second-order focusing. The results of measurements of the focusing properties will also be reported.

I. Focusing and resolving power

a) Graphical construction

The conventional sector field with perpendicular entrance and exit of the ion beam gives the image of the entrance slit on the line through this slit and the centre of curvature of the ion beam (Barber's rule). When the beam does not cross the field boundaries perpendicularly, we may construct the focus in the following way, which has been given by CARTAN [9].

Fig. 1 A shows how the focus is displaced along the central beam, when the angle ε between the central beam and the normal of the boundary varies. When crossing the line 00′ the three indicated beams are parallel (the distances between the beams are greatly exaggarated in the figure). They are then focused at the point F_0, if the angle $\varepsilon = 0$, i.e. normal exit. If $\varepsilon \neq 0$, they

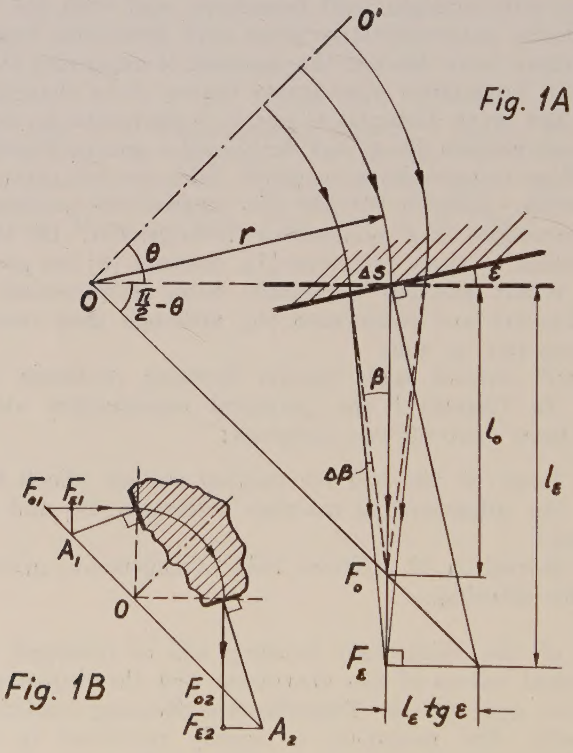

Fig. 1 A. Variation of the focal displacement with the angle ε. B. Graphical construction for the focal point, for arbitrary angle of incidence.

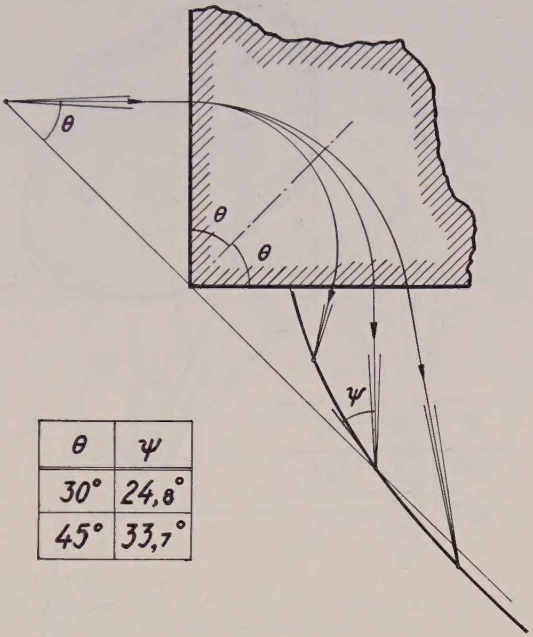

Fig. 2. The locus of the foci for varying radius of curvature, with straight field boundaries. The arrows give the directions of the ion beams. The angle ψ has been calculated according to the formula given in Table 1.

will have the focal point F_ε. When $\Delta s \ll r$ we get from Fig. 1 A that $\beta = \Delta s / l_0$, $\Delta \beta = \Delta s \cdot \operatorname{tg} \varepsilon / r$ and $\beta - \Delta \beta = \Delta s / l_\varepsilon$ and then

$$\frac{l_\varepsilon - l_0}{l_0} = \frac{l_\varepsilon \cdot \operatorname{tg} \varepsilon}{r}. \tag{1}$$

By means of Eq. (1) and making use of the properties of similar triangles, the graphical construction can be done as follows, where index 1 is reserved for the entrance side and index 2 for the exit (image) side (see Fig. 1 B). A perpendicular to the median ion beam through the point $F_{\varepsilon 1}$, the entrance slit, crosses the normal to the field boundary in the point A_1. The line through A_1 and O, the centre of curvature of the median ion beam, will cross the normal to the field boundary of the exit side in A_2. The focus point $F_{\varepsilon 2}$ is now obtained by drawing a perpendicular to the median beam through A_2. This construction has been used to obtain different loci of the foci, as shown in Figs. 2–6.

In Fig. 2 we see the locus of the foci for different masses, when the field boundaries are straight and the angle of the apex is 90°. It appears that different masses in a mass spectrometer will in general not be focused on the straight line through the apex of the field and the entrance slit, as is sometimes said in the literature. For a special case with circular boundaries the locus is shown in Fig. 3. The angle ψ is defined as the angle between the

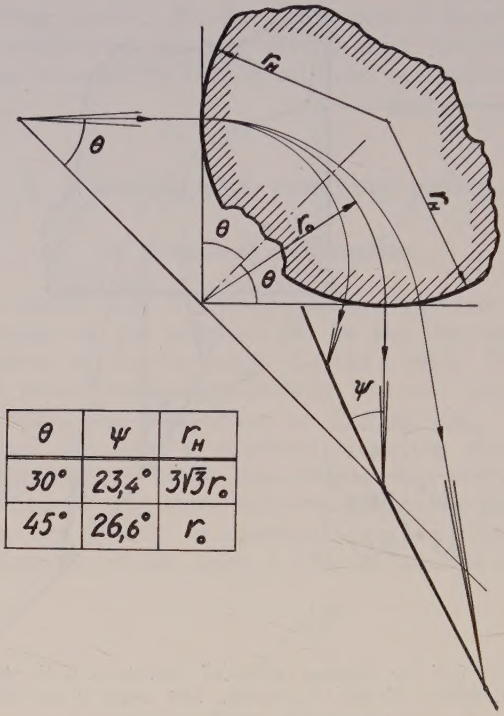

θ	ψ	r_H
30°	23,4°	$3\sqrt{3}r_0$
45°	26,6°	r_0

Fig. 3. The same construction as in Fig. 2, but for circular boundaries.

tangent of the locus and the central beam. The numerical values of ψ given in these figures are calculated according to formulae shown later.

The directional focusing properties of the normal $\pi/2$-type and the type with circular boundaries are shown in Figs. 4 and 5. In both cases the aberration will have a minimum for beams which are focused in the turning point of the locus. Thus we see that the best focusing for the straight boundaries is obtained for $\alpha = \alpha_0$ (α is defined in Fig. 4), which is the so-called "inflection case" [5]. With circular boundaries, on the other hand, the smallest aberration occurs for $\alpha = 0$.

From such curves as constructed in Figs. 4 and 5 it is possible to estimate the aberration. Assuming in Fig. 5 that $\alpha = dy_2/dx_2$ for the beam and that $r_0 - x_2 = C\alpha^2$ (where C = constant) for the locus, it can be shown that the aberration is $(C/6)\alpha^3$, when the beam is symmetrical around $\alpha = 0$. From the curve to the left we estimate C to be about $6 \cdot r_0$ and thus the aberration is about $r_0\alpha^3$. This is to be compared with the aberration $r_0\alpha^2$ in the case of wedge-shaped fields (as in Fig. 4, when $\alpha = 0$ for the median beam).

A further refinement giving third-order focusing is shown in Fig. 6. The deflection of the beam for the best focusing is, however, greater than $\pi/2$ ($\approx 107.5°$).

It is obviously the curvature of the field boundary which is responsible for the aberration and the angle ψ, while the tangent to the field boundary gives

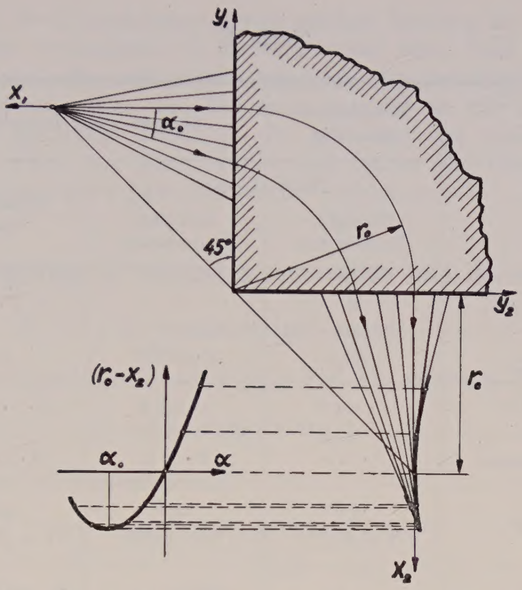

Fig. 4. The locus of the foci for varying angle of incidence with constant radius of curvature. Straight boundaries. (The angle $\alpha_0 = 16°$).

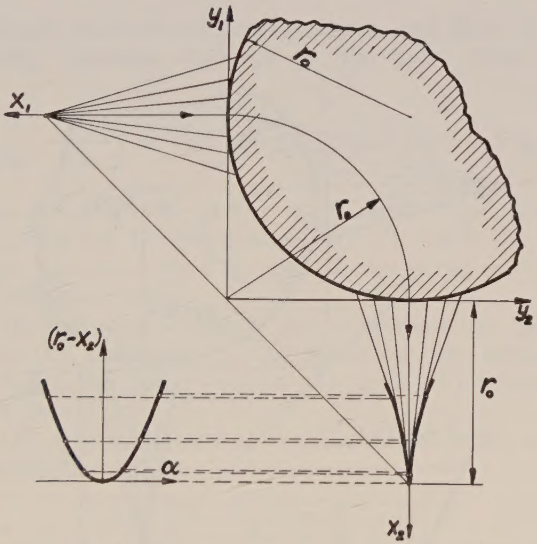

Fig. 5. The same construction as in Fig. 4, but for circular boundaries.

the focus point and the dispersion (compare Fig. 2 with Fig. 3 and Fig. 4 with Fig. 5 and see also Table 1). A closer investigation shows that straight boundaries give second-order focusing at most, while circular boundaries can give third-order focusing as shown in Fig. 6. This can be seen by a comparison with the

Table 1.

	First-order focusing	Second-order focusing	
	Normal case		Inflection case
	Straight boundaries	Circular boundaries	
$\mathrm{tg}\,\varepsilon$	0	0	$-\frac{1}{2}\cdot\mathrm{tg}\,\theta$
r_H	∞	$r\cdot\cot^3\theta$	∞
l	$r\cdot\cot\theta$	$r\cdot\cot\theta$	$\frac{2}{3}\cdot r\cdot\cot\theta$
Dispersion	$2\cdot\Delta r$	$2\cdot\Delta r$	$\frac{2}{3}\cdot 2\cdot\Delta r$
$\mathrm{tg}\,\psi$	$\dfrac{\mathrm{tg}\,\theta}{1+\sin^2\theta}$	$\dfrac{\mathrm{tg}\,\theta}{1+\mathrm{tg}^2\,\theta}$	$\dfrac{\mathrm{tg}\,\theta}{1+\frac{1}{2}\cdot\mathrm{tg}^2\,\theta}$
Aberration	$r\,\alpha^2$	$\dfrac{\cot\psi}{2}\cdot r\,\alpha^3$	$\dfrac{2}{3}\cdot\dfrac{\cot\psi}{2}\cdot r\,\alpha^3$

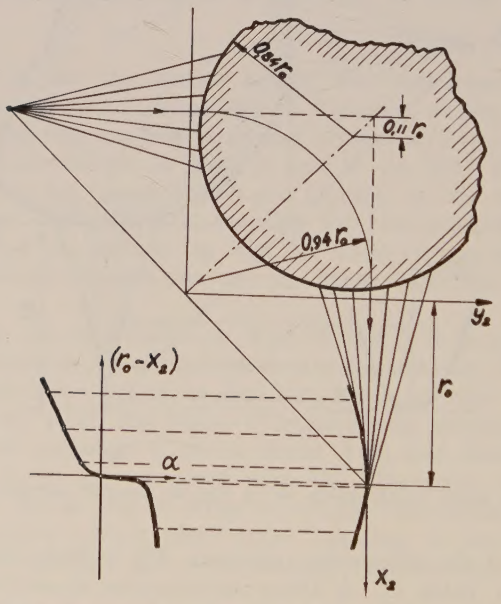

Fig. 6. An example of third-order focusing. The deflection of 107.5° gives minimum aberration.

shape of the ideal field boundaries giving perfect focusing as shown by HINTENBERGER [2]. If the boundaries of a symmetrical ideal field are approximated at the entrance and the exit of the ion beam by circular boundaries having the same radius of curvature and the same tangent as the ideal field, second-order focusing is generally obtained. In one case we also have third-order focusing, namely when the beam enters and leaves the ideal field across the points where its boundaries have maximum curvature.

b) Calculations of dispersion, aberration and the angle ψ

1) Symmetrical cases

If we write $l_\varepsilon = l$ and $l_0 = r \cdot \cot \theta$ (see Fig. 1), equation (1) gives

$$l = r/(\operatorname{tg} \theta - \operatorname{tg} \varepsilon). \tag{2}$$

From this we have by differentiation

$$\frac{d\,l}{l} = \frac{d\,r}{r} - \frac{d\,\theta/\cos^2\theta - d\,\varepsilon/\cos^2\varepsilon}{\operatorname{tg}\theta - \operatorname{tg}\varepsilon}. \tag{3}$$

Applying (2) and (3) to both halves of a magnetic lens, it is possible to calculate the second-order aberration and the dispersion and also the angle ψ (see Fig. 7).

By means of simple geometrical considerations and Eqs. (2) and (3) we obtain the *second-order focusing condition* in the case, when $\theta_1 = \theta_2 = \theta$ and $\varepsilon_1 = \varepsilon_2 = \varepsilon$:

$$r\left(\frac{1}{r_{H1}} + \frac{1}{r_{H2}}\right) = 2\cos^3\varepsilon\,(\operatorname{tg}\theta - \operatorname{tg}\varepsilon)^2\,(\operatorname{tg}\theta + 2\operatorname{tg}\varepsilon) \tag{4}$$

where r_{H1} and r_{H2} are the radii of curvature of the field boundaries. Eq. (4) has already been given by HINTENBERGER [4]. If $\varepsilon = 0$ (*the normal case*) and $r_{H1} = r_{H2} = r_H$, we get $r_H = r\cot^3\theta$, and if $r_{H1} = r_{H2} = \infty$, we have $\operatorname{tg}\varepsilon = -(\tfrac{1}{2})\operatorname{tg}\theta$ (*the inflection case*).

The results of further calculations on the *aberration* are collected in Table 1. The expression for the aberration in the inflection case given by KERWIN [5] seems to be four times too large because the focal displacement has not been taken into account (see Fig. 4).

The *dispersion* (D) measured normal to the central beam is for symmetrical cases found by calculation to be

$$D = 2\,\Delta r \cdot \operatorname{tg}\theta/(\operatorname{tg}\theta - \operatorname{tg}\varepsilon) \tag{5}$$

where $\Delta r \ll r$. If A is the mass-to-charge ratio, we can write $2 \cdot \Delta r = r \cdot \dfrac{\Delta A}{A}$. For the normal case (index n) we have $D_n = 2 \cdot \Delta r$ and for the inflection case (index f) $D_f = (\tfrac{2}{3}) \cdot 2 \cdot \Delta r$. Thus we obtain the constant ratio $D_f : D_n = \tfrac{2}{3}$. (This result is to be compared with that in [5], which is calculated using wrong assumptions.)

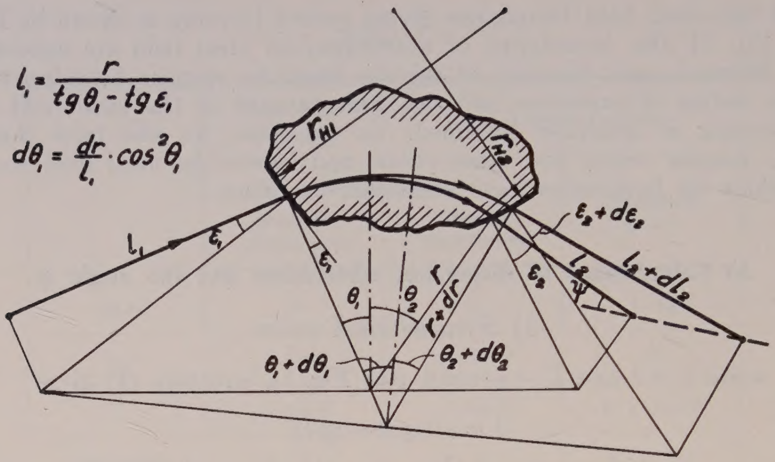

$$d\theta_2 = -\frac{dr}{r}\left\{\sin(\theta_1+\theta_2) + tg\,\varepsilon_2\left[1-\cos(\theta_1+\theta_2)\right]\right\} - d\theta_1$$

$$d\varepsilon_2 = \frac{dr}{r} \cdot \frac{1-\cos(\theta_1+\theta_2)}{\cos\varepsilon_2} + d\theta_1 + d\theta_2$$

Fig. 7. Method for the calculation of the dispersion and the angle ψ.

The calculation of *the angle* ψ is demonstrated in Fig. 7, and the results are given in Table 1. A few numerical values are given in Figs. 2 and 3. In the case of second-order focusing, we see that the maximum value of ψ corresponds to minimum aberration. We obtain

$\psi_{n\,\max} = 26.6^\circ$ ($\theta = 45^\circ$) and

$\psi_{f\,\max} = 35.3^\circ$ ($\theta = 54.7^\circ$, $\theta + |\varepsilon| = 90^\circ$ and thus we have a 180°-magnet).

The calculation of the *third-order focusing condition* is rather laborious even for the symmetrical cases. It may however be shown that the arrangement in Fig. 6 has the following values for the third-order focusing: $\theta = 53.8^\circ$, $\varepsilon = 28.6^\circ$ and $r_H = 0.89\, r$. From this it is possible to calculate the values given in Fig. 6. The value of ψ, which is of interest when discussing the resolving power, is found by the graphical method to be about 22°.

2) Asymmetrical cases

In asymmetrical cases ($\theta_1 \neq \theta_2$, $\varepsilon_1 \neq \varepsilon_2$), the formulae are generally more complicated. But one case that might be of interest is when $r_{H1} = r_{H2} = \infty$, $\varepsilon_1 = 0$ and $\theta_1 = \theta_2 + |\varepsilon_2|$, i.e. there are straight field boundaries and normal incidence but oblique exit of the beam. (These conditions have already been discussed by Kerwin and Geoffrion [6]. Their results are, however, not correct, because their assumption is valid only when $\theta_1 = \theta_2$ and $\varepsilon_1 = \varepsilon_2$.) The second-order focusing condition is now

$$\sin^3 \theta_1 = (1 + k)^2 \cdot (2\,k - 1) \cdot \sin^3 \theta_2 \tag{6}$$

where

$$k = -\operatorname{tg} \varepsilon_2 / \operatorname{tg} \theta_2. \tag{7}$$

This condition may also be found by using the general equation given by HINTENBERGER [4].

Table 2.

θ_1	θ_2	ε_2	l_2	D	M	ψ
30°	11.5°	−18.5°	$1.86 \cdot r$	$0.66 \cdot 2 \cdot \Delta r$	0.95	21.5°
45°	19.3°	−25.7°	$1.20 \cdot r$	$0.66 \cdot 2 \cdot \Delta r$	0.90	29.9°
90°	47.0°	−43.0°	$0.50 \cdot r$	$0.63 \cdot 2 \cdot \Delta r$	0.73	31.7°

In Table 2 the results are given for $\theta_1 = 30°$, 45°, and 90°. There we also find the values of the distance l_2 and the dispersion (D) as well as the magnification (M), which is of interest when calculating the resolving power. D and M are given by the following equations

$$D = 2 \cdot \Delta r \cdot (\tfrac{1}{2}) \cdot [1/(1 + k) + \cos \varepsilon_2] \tag{8}$$

$$M = [(2\,k - 1)/(1 + k)]^{\frac{1}{3}} \tag{9}$$

The angle ψ is also calculated and the result is found in the table.

c) The fringe field

Hitherto we have not taken the fringe field into account. But even if we have a fringe field in Figs. 4 and 5 there will be a locus of the foci having a form such that second-order focusing appears at some point. We can say that we have an effective field boundary and usually it will lie outside the boundary of the pole pieces at a distance of about the width of the pole gap. This is true for the ion beams in a certain plane, but because of the curvature of the fringe field different parallel planes have different effective field boundaries. Thus the image of the entrance slit will be curved [12]. To suppress this effect we have to use slits which are not too long in comparison with their widths. (The length of the slits will also introduce another broadening effect, because beams not parallel to the median plane will have their velocity perpendicular to the magnetic field diminished.) In practice the optimum conditions for a given magnet and analyzer tube are achieved by adjusting the magnet relatively to the tube and, if possible, by varying the direction of the ion beam.

d) Resolving power

We consider the case when there is one fixed collector. If the width of the collector slit is vanishingly small, we would measure the intensity distribution in the beam. On the other hand if the width of the collector slit is greater than the width of the beam, the measured peak has a flat top. That is what

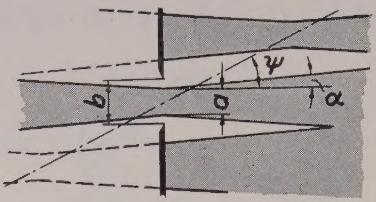

Fig. 8A

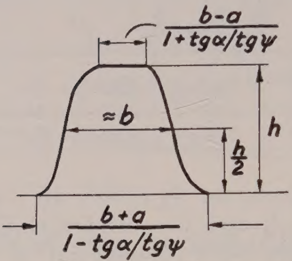

Fig. 8B

Fig. 8 A. The beams in the neighbourhood of the collector slit.
B. The measured peak, when $b > a$.

is wanted for abundance measurements with a mass spectrometer and what is considered in the following.

The fact that the angle ψ is generally less than 90° (see Table 1 and Figs. 2 and 3), has the effect that the base of a peak is broadened and its flat top diminished with descreasing values of the angle ψ. When the plate with the slit is perpendicular to the central beam, we find from Fig. 8 that the base and the top are

$$\frac{b + a}{1 - \operatorname{tg} a/\operatorname{tg} \psi} \quad \text{and} \quad \frac{b - a}{1 + \operatorname{tg} a/\operatorname{tg} \psi}$$

respectively, where a = the image width, b = the width of the collector slit and α = the half angle of divergence of the beam on the image side (in symmetrical cases this angle is the same on both the sides of the magnetic lens). The half-value width may be different from b depending on the intensity distribution. The given expressions of the base and the top are not quite correct, when there is only first-order focusing, because the image is not perpendicular to the central beam in this case. Instead of a we have to write $a\,(1 - \sin 2\,\theta \operatorname{tg} \alpha)$ and $a\,(1 + \sin 2\,\theta \operatorname{tg} \alpha)$ resp.

To resolve two neighbouring peaks it is necessary that the dispersion should at least be as large as the base of one peak, i.e. the following inequality must be satisfied:

$$p \cdot r \cdot \frac{\Delta A}{A} \geq \frac{b + a}{1 - \operatorname{tg} a/\operatorname{tg} \psi}, \tag{10}$$

where A = the mass-to-charge ratio, ΔA = the difference in A ($\Delta A \ll A$) and p = a factor depending on the arrangement ($p_n = 1$, $p_f = \frac{4}{3}$, see Table 1). Further we have

$$a = M a_0 + p \cdot r \cdot (\Delta E/E) + \Delta a, \tag{11}$$

where a_0 = the entrance slit width, M = the magnification, $\Delta E/E$ = the relative energy spread and Δa = the broadening not depending on the energy spread or the angle ψ. The *resolving power* is defined as

$$\left(\frac{A}{\Delta A}\right)_{\max} = \frac{p \cdot r}{a + b} \cdot (1 - \operatorname{tg} \alpha / \operatorname{tg} \psi), \tag{12}$$

and when $b - a \ll a$ we obtain

$$\left(\frac{A}{\Delta A}\right)_{\max} \approx \frac{p \cdot r\,(1 - \operatorname{tg} \alpha / \operatorname{tg} \psi)}{2\,(M a_0 + p r \cdot \Delta E/E + \Delta a)}. \tag{13}$$

From Eq. (13) can be seen that

1) with great energy spread, i.e. when $p \cdot r \cdot \Delta E/E \gg M_0 + \Delta a$, the resolving power is independent of p,

2) when $M a_0 \gg p r \cdot \Delta E/E + \Delta a$, we find $(A/\Delta A)_{\max}$ to be proportional to p,

3) when having the commonly used first-order focusing and a relatively great divergence of the beam, i.e. $\Delta a \approx r \alpha^2 \gg M a_0 + p r \cdot \Delta E/E$, we obtain

$$\left(\frac{A}{\Delta A}\right)_{\max} \approx \frac{1 - \operatorname{tg} \alpha / \operatorname{tg} \psi}{2\,\alpha^2}.$$

When there is second-order focusing, the influence of the third-order aberration may be neglected. But the divergence of the beam has nevertheless a broadening effect through the factor $(1 - \operatorname{tg} \alpha / \operatorname{tg} \psi)$. If $\alpha = 4^\circ$ and $\operatorname{tg} \psi = 0.5$, we obtain $\operatorname{tg} \alpha / \operatorname{tg} \psi = 0.14$, i.e. a decrease of 14 % in the resolving power.

A comparison between the normal case with circular boundaries and the inflection case shows that with the same values of r and θ (the same ion path in the magnetic field), the former case will give a greater resolving power than the latter case, because $p_n = 1$ and $p_f = \frac{2}{3}$, but at the same time the ion path will increase with $(\frac{2}{3}) \cdot r \cdot \cot \theta$ (see Table 1). From Table 1 we also see that the angle ψ of the inflection case is greater than that of the normal case, but this difference will have negligible influence on the resolving power, if $\alpha < 5^\circ$.

The special case of third-order focusing shown in Fig. 6 has $\operatorname{tg} \alpha / \operatorname{tg} \psi \approx 2.5\,\alpha$. When $\alpha = 5^\circ$, we get $1 - \operatorname{tg} \alpha / \operatorname{tg} \psi = 0.78$. Thus the resolving power may decrease appreciably with increasing α, even though the third-order aberration is negligible.

The influence of the factor $\operatorname{tg} \alpha / \operatorname{tg} \psi$ can be diminished by turning the plate with the collector slit so that the angle between the plate and the central beam is less than 90° and about equal to ψ.

II. Practical application of the theory

a) The instrument

A mass spectrometer constructed to give second-order focusing has been built. A block scheme of the instrument is shown in Fig. 9.

The pole pieces are constructed for normal incidence of the ion beam ($\varepsilon = 0$). According to the formula in Table 1 we would in this case ($\theta = 45°$) have $r_H = r$, i.e. the field boundary has the same radius of curvature as the median ion beam. To correct for the fringe field we have reduced r_H with the width of the pole gap (see I c). The radius of curvature of the median ion beam is 150 mm, the pole gap 15 mm and thus the value of r_H is 135 mm (see Fig. 10). For symmetrical fields when $\varepsilon = 0$ BAINBRIDGE [1] has given the formula $r_H = r \cos^2 \theta \ (\cos \theta - \alpha)$, where α is the half angle of divergence. In what way he has derived this formula is unknown by the author. The correction for α goes, however, in the same direction as the fringe field correction performed here.

The analyzing chamber is made of a copper tube, flattened to fit in the pole gap without touching the pole pieces. Round the free ends of the tube there are wire windings as heating elements, delivering an effect of 350–400 watts when baking the analyzer. Both ends of the tube are sealed by cooled rubber gaskets. The electrical connections are made by means of Kovar-glass seals.

The ion source is to a great extent a copy of NIER's [13], but we have the possibility of analyzing solid as well as gas samples. This is possible by means of the device shown in Fig. 11. When analyzing solid samples the centre part has an oven and a crucible of platinum. Without spoiling the vacuum in the analyzer we are able to change the centre part and introduce new samples. For gas analyses, on the other hand, we have a capillary leak.

On the exit side we have only a single collector, and the measurements are performed by scanning the high voltage. The spectrum is then registered by a recorder (Speedomax). The scanning can be done either 1) by varying the

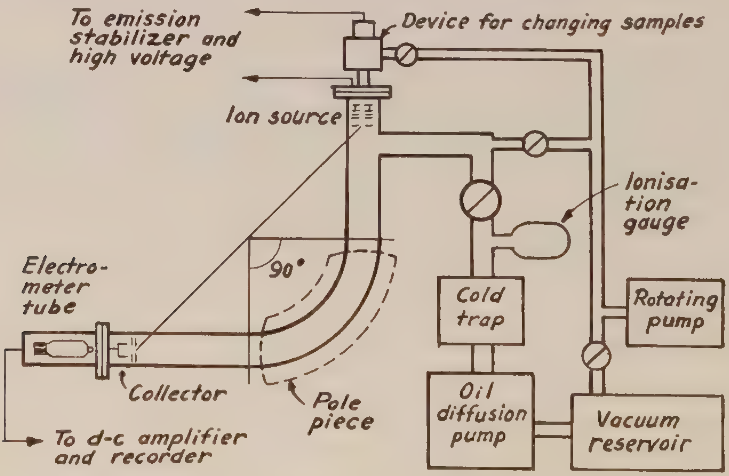

Fig. 9. Block diagram of the mass spectrometer.

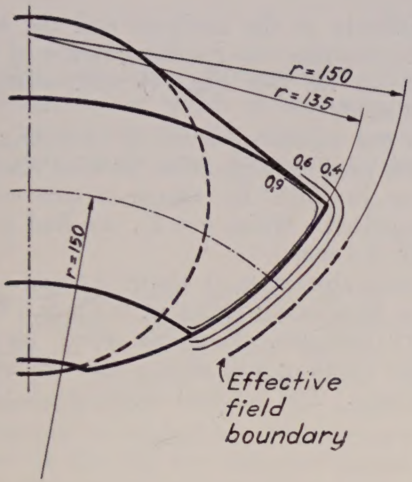

Fig. 10.

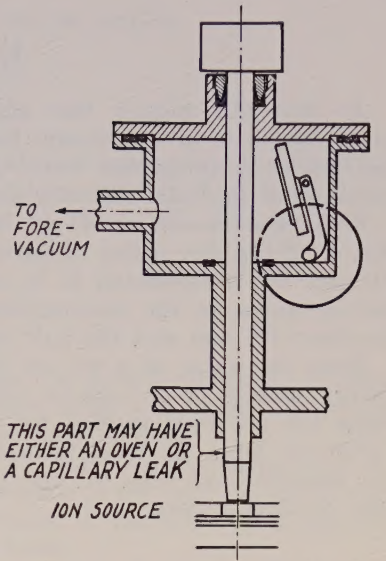

Fig. 11.

Fig. 10. The pole piece. The figures 0.9, 0.6 and 0.4 give the field strength at the edge compared with that of the homogeneous field.

Fig. 11. The device for changing samples.

reference voltage (E_0 in Fig. 12) or 2) by changing with constant speed the position of the grid contact of the potentiometer R (Fig. 12). We have $xE = E_0$ and for voltage scanning the product $A\,E$ is constant. Thus it follows that A is a linear function of x and in case 2) we get a linear mass scale on the recorder.

The emission stabilizer and the amplifier are mainly copied from the work of Graham, Harkness and Thode [14]. As preamplifier we have used the electrometer tube FP 54.

The current for the magnet is taken from a heavy duty battery, and the magnetic field is 7 000 gauss, when the current is 2 A. Thus at an energy of 1 500 V it is possible to collect masses up to 350.

Fig. 12 A

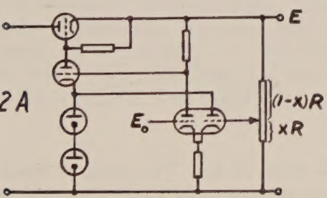

Fig. 12 B

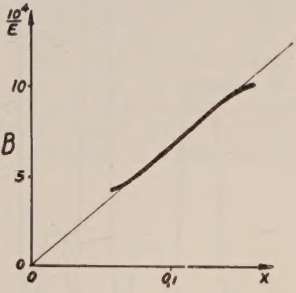

Fig. 12 A. Schematic circuit of the high-voltage scanning unit. B. Variation of high voltage with position of scanning potentiometer.

b) Focusing test

At first the magnet was adjusted relatively to the analyzer and the slits were aligned to give optimum focusing. To examine the resolving power of the instrument spectrograms were then taken on Zn (see Fig. 13) with entrance slit $5 \times 0.3\ \text{mm}^2$ and collector slit $5 \times 1.\ 3\ \text{mm}^2$.

From the spectrograms we can obtain the values of a and b according to Fig. 8. When the radius of curvature is 150 mm, the dispersion between masses 64 and 66 is calculated to be 4.6 mm (see Eq. (5)). By means of this value the distances in the spectrogram are normalized. When $\alpha \approx 2^\circ$, we find a to be about 0.7 mm and the half value width 1.4 mm.

From the value of a we see that the total aberration is about 0.4 mm. An energy spread of 2 volts in 1 500 gives a broadening effect of 0.2 mm. This value has not been verified but seems very probable. Assuming $\alpha = 2^\circ$ we get $r\,\alpha^3 = 0.01$ mm. An incomplete second-order focusing will give a greater value, but certainly less than 0.1 mm ($r\,\alpha^2 = 0.2$ mm). The residual aberration is then due to other causes.

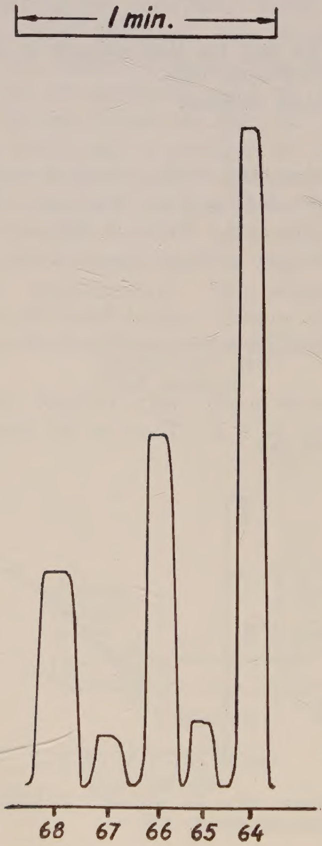

Fig. 13. Spectrum of Zn. The peak at mass 65 ($C_5H_5^+$) is due to the pump oil (the cold trap not in use). It is asymmetrically placed between the Zn-peaks 64 and 66 because of the great difference in mass defects.

According to Eq. (12) the resolving power can be written

$$\frac{150\,(1 - \mathrm{tg}\,\alpha/\mathrm{tg}\,\psi)}{0.7 + 1.3}.$$

In this case $\mathrm{tg}\,\psi = 0.5$ and $\mathrm{tg}\,\alpha \approx 0.035$. Thus the resolving power should be 70.

Reducing the width of the entrance slit to 0.1 mm and that of the collector slit to 0.6 mm would give a resolving power of about 127. The flat top of the peak would then be about 0.1 mm.

SUMMARY

1) The graphical construction by CARTAN (see I a) is very convenient to show the focusing properties of homogeneous magnetic fields and, according to the opinion of the author, this method ought to be more known.

2) The influence of the beam divergence on the resolving power may be rather important, even if the second-order aberration is zero and the third-order aberration is negligible. This depends on the value of the angle ψ between the locus of the foci for different masses and the beam.

3) Second-order focusing may be obtained by using either the normal case with circular boundaries or the inflection case. Assuming the same ion path in the magnetic field, the resolving power in the former case is greater, but the total ion path longer than in the latter case.

Acknowledgements

I wish to express my sincere thanks to the director of the physical department, Dr. S. EKLUND, for his encouraging interest and to Dr. N. SVARTHOLM for advice and helpful discussions. My thanks are also due to Cand. real. H. v. UBISCH for valuable suggestions and to Mr. L. HEDLUND and Mr. Y. CARLSSON for technical assistance.

A.B. Atomenergi, Department of Physics, Stockholm.

REFERENCES: [1] **K. T. Bainbridge,** VII^{e} Conseil de Chimie Solvay 1947, p. 55. — [2] **H. Hintenberger,** Z. Naturforschg *3 A,* 125 (1948). — [3] ——, Z. Naturforschg *3 A,* 669 (1948). — [4] ——, Rev. Sci. Inst. *20,* 748 (1949). — [5] **L. Kerwin,** Rev. Sci. Inst. *20,* 36 (1949). — [6] ——, **C. Geoffrion,** Rev. Sci. Inst. *20,* 381 (1949). — [7] ——, Rev. Sci. Inst. *21,* 96 (1950). — [8] **M. Spighel,** J. de Phys. Rad., Série VIII, *10,* 207 (1949). — [9] **M. L. Cartan,** J. de Phys. Rad., Série VII, *8,* 453 (1937). — [10] **J. A. Hunter, R. W. Stacy, F. A. Hitchcock,** Rev. Sci. Inst. *20,* 333 (1949). — [11] **L. G. Lewis, R. J. Hayden,** Rev. Sci. Inst. *19,* 599 (1948). — [12] **W. Ploch, W. Walcher,** Z. Physik *127,* 274 (1950). — [13] **A. O. Nier,** Rev. Sci. Inst. *18,* 398 (1947). — [14] **B. L. Graham, A. Harkness, H. G. Thode,** J. Sci. Inst. *24,* 119 (1947).

Tryckt den 10 september 1951

Uppsala 1951. Almqvist & Wiksells Boktryckeri AB